

Optimisation of the CBM magnetic field

Facility for Antiproton and Ion Research in Europe and
GSI Helmholtzzentrum für Schwerionenforschung

WIOLETTA BORZYM



Internship and Training Project Report
Darmstadt, Germany
September-2019

GET INvolved 2018: THXXX (GI18-TH-XXX)

Copyrights(c)

Personal use of this material is permitted. However, permission to reprint/republish this material for advertising or promotional purposes or for creating new collective works for resale or redistribution to servers or lists, or to reuse any copyrighted component of this work in other works must be obtained from the GSI GmbH and FAIR GmbH.

Author

Wioletta Borzym

Warsaw University of Technology, Faculty of Physics

00-662 Warsaw, ul. Koszykowa 75, Warsaw - Poland

Email: wiola.borzym@gmail.com

Project Mentor/Supervisor

Dr. Volker Frieze

CBM

GSI Helmholtzzentrum für Schwerionenforschung GmbH,

Planckstr. 1, 64291 Darmstadt, Germany

Tel: +49 6159 71 1619

Email: email@gsi.de

Program Coordinator

Dr. Pradeep Ghosh

GSI Helmholtzzentrum für Schwerionenforschung GmbH &

Facility for Antiproton and Ion Research in Europe GmbH

Tel: +49 6159 71 3257, Fax: +49 6159 71 3916

Email: Pradeep.Ghosh@fair-center.eu

GET Involved 2019: yzzz

Publisher: GSI Helmholtzzentrum für Schwerionenforschung GmbH,

Planckstr. 1, 64291 Darmstadt, Germany

Published: September 2019

Declaration

I hereby declare that the project entitled "**Optimisation of the CBM magnetic field**" is my own work and that I have correctly acknowledged the work of others.

Acknowledgements

I want to thank for the opportunity of internship in GSI, as it was a great chance for improvement of my skills and professional development. Also, I am very grateful for a chance to meet many excellent people from all over the world and professionals who helped me with my work.

I want to express my gratitude to Dr.Volker Friese for providing me with advices and knowledge, for guidance and for motivating me to always give my best and to believe in myself.

I hope to use the gained skills in my future career in physics. I will continue to work on improving them.

I hope to continue cooperation with GSI in the future.

Abstract

CBM will measure collisions at various beam momenta and is not clear which magnetic field settings are optimal for the various beam momentum. By studying key CBM observables: geometrical acceptance, reconstruction efficiency, momentum resolution, Lambda reconstruction and Lambda efficiency the best field settings can be found.

By studying the impact of the magnetic field settings for key performance figures of CBM we learned that magnetic field has no significant influence on geometrical acceptance of primary protons.

We have more reconstructed momentum values for lower magnetic field but momentum resolution increases from 2% to about 5% when reducing the magnetic field for the same beam momentum.

The distribution of invariant mass of Lambda cannot be done properly without the extrapolation of the reconstructed momentum to the decay point.

Lambda reconstruction efficiency is higher for lower beam momentum and is higher when reducing magnetic field.

The width of Lambda peak increases when reducing the field but stays almost the same for different beam momentum and the same magnetic field setup.

Signal-to-background ratio drops when reducing the field by a factor of 2 and for lower magnetic field settings the ratio approaches unity.

Contents

1	Introduction	10
1.1	CBM Experiment	10
1.2	The CBM Setup	10
2	Geometrical acceptance	12
3	Reconstruction efficiency	15
4	Momentum resolution	17
5	Lambda reconstruction	19
6	Lambda efficiency	23
7	Conclusion	27

List of Figures

1.1	QCD Phase Diagram of strongly interacting matter	10
1.2	CBM Setup	11
1.3	STS and TOF scheme. We accept particle as a candidate to our calculations only if it has at least 4 STS points and 1 TOF point.	11
2.1	Rapidity distribution for 12GeV/u and 100 % magnetic field	12
2.2	Rapidity distribution of protons for 4GeV/u and 100 % magnetic field	13
2.3	Rapidity distribution of protons accepted in STS and TOF for 4GeV/u and different magnetic field settings	13
2.4	Distribution of accepted protons in transverse momentum and rapidity 4 GeV/u beam momentum and different magnetic field settings	14
2.5	TOF acceptance for 4GeV/u beam momentum and different magnetic field settings	14
3.1	Momentum distribution for 12GeV/u beam momentum 100% magnetic field for all simulated primary protons and all reconstructed primary protons	15
3.2	Momentum distribution for 4GeV/u beam momentum 100% magnetic field for all simulated primary protons and all reconstructed primary protons.	16
3.3	Momentum distribution for 4GeV/u beam momentum and different magnetic field settings for reconstructed primary protons	16
4.1	2D histogram of dp/p in function of momentum for primary protons	17
4.2	Example of projection of the dp/p(p) distribution with Gaussian fit	18
4.3	Relative momentum resolution as function of momentum for different beam momentum and 100% of magnetic field	18
4.4	Relative momentum resolution as function of momentum for 4GeV/u beam momentum and different settings of magnetic field	18
5.1	Distribution of invariant mass of Lambda with use of Monte Carlo data	19
5.2	Impact parameter	20
5.3	Impact parameter distribution for primary and secondary protons	20
5.4	Impact parameter distribution for primary and secondary π^-	21
5.5	m^2 distribution as function of momentum for primary π^- and protons	21
5.6	Distribution of invariant mass of $p\pi^-$ with the reconstructed momentum	22
5.7	Distribution of invariant mass of $p\pi^-$ with Monte Carlo momentum values	22
6.1	Efficiency of Lambda for different beam momentum and 100% of magnetic field	23
6.2	Efficiency of Lambda for 4GeV beam momentum and different magnetic field settings	24
6.3	Reconstructed invariant mass of Lambda from KFParticle Finder with Gaussian fit	24

6.4	Width of the Lambda peak for different energies and different magnetic field settings	25
6.5	Distribution of invariant mass of $p\pi^-$ from KFParticle Finder. The marked area under the peak is the background used for calculating the signal-to-background ratio.	25
6.6	Signal to background ratio as function of beam energy for different magnetic field settings	26

Chapter 1

Introduction

1.1 CBM Experiment

The Compressed Baryonic Matter (CBM) experiment is still under the construction. The main aim of the CBM experiment is to explore the QCD phase diagram in the region of high baryon densities using high-energy nucleus-nucleus collisions. By that we can study the equation-of-state of nuclear matter at neutron star core densities and phase transitions. The CBM setup is designed to measure the collective behavior of hadrons with unprecedented precision and statistics. To achieve that the measurements will be performed at reaction rates up to 10 MHz. CBM will measure collisions at various beam momenta (2 – 12 GeV/u). The CBM experiment will deliver a proper conditions for substantial discovery potential for fundamental properties of QCD matter.[1]

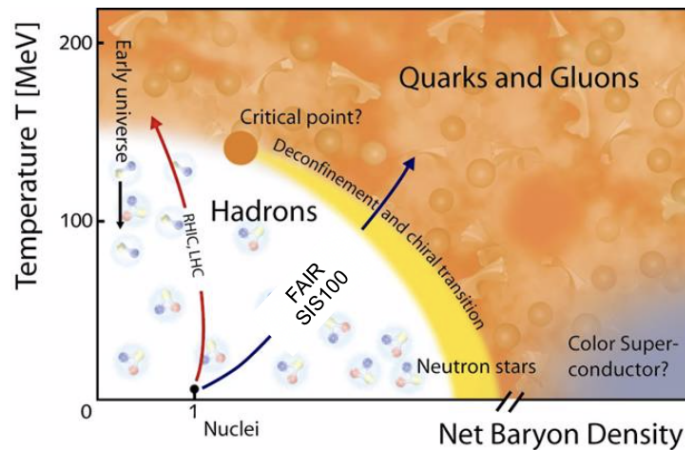


Figure 1.1: QCD Phase Diagram of strongly interacting matter

1.2 The CBM Setup

The CBM setup comprises several high-performance detector systems: Micro-Vertex Detector (MVD), Silicon Tracking System (STS), both placed in a super-conducting magnet, Muon Chamber System (MUCH), Transition Radiation Detectors (TRD), Resistive Plate Chambers for time-of-flight measurements (TOF) and Projectile Spectator Detector (PSD). The dipole magnet bends the trajectory of charged particles in order to calculate their momenta.

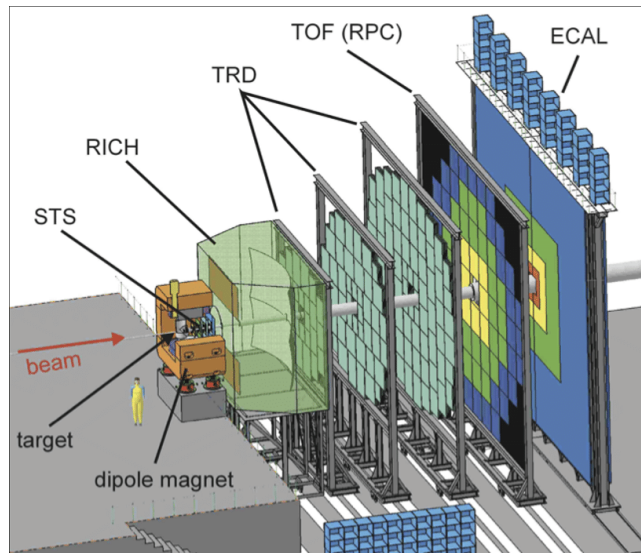


Figure 1.2: CBM Setup

The Silicon Tracking System is one of the main detectors of the CBM experiment. It will provide track reconstruction and momentum determination for charged particles. The STS consists of 8 tracking stations made of silicon detectors.

The time-of-flight detector will provide measurements which will be used for charged particle identification. The particle mass can be calculated having the time of flight, the momentum of the particle and the track length.[2]

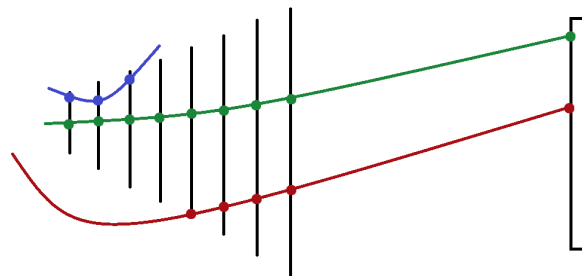


Figure 1.3: STS and TOF scheme. We accept particle as a candidate to our calculations only if it has at least 4 STS points and 1 TOF point.

CBM uses a dipole magnet to determine the charged-particle momenta from their curvature in the magnetic field. It is possible to scale the magnetic field by adjusting the current in the magnet.

CBM will measure collisions at various beam momenta (2 – 12 GeV/u). It is yet not clear which magnetic field settings are optimal for the various beam momentum. Changing the field strength and other performance figures will lead to a change in the acceptance, but also affects the momentum resolution and other performance figures of the spectrometer.

We can study key CBM observables by simulation at different collision energies and varying the magnetic field settings. The best field settings are to be found by optimising the CBM performance (acceptance, efficiency, resolution) for these key observables.

Chapter 2

Geometrical acceptance

One of the main values used for analysis in physics is rapidity, used as a measure for relativistic velocity in relative physics.

$$y = \frac{1}{2} \ln \frac{E + p_z}{E - p_z} \quad (2.1)$$

In every one of the later calculation I take the value of the speed of light $c=1$.

We want the distribution of rapidity to be symmetrical with respect to midrapidity line, which is defined as half of the beam rapidity. Particles which were used in thi analysis are protons because they have the highest statistics and are charged, so we can detect them in CBM.

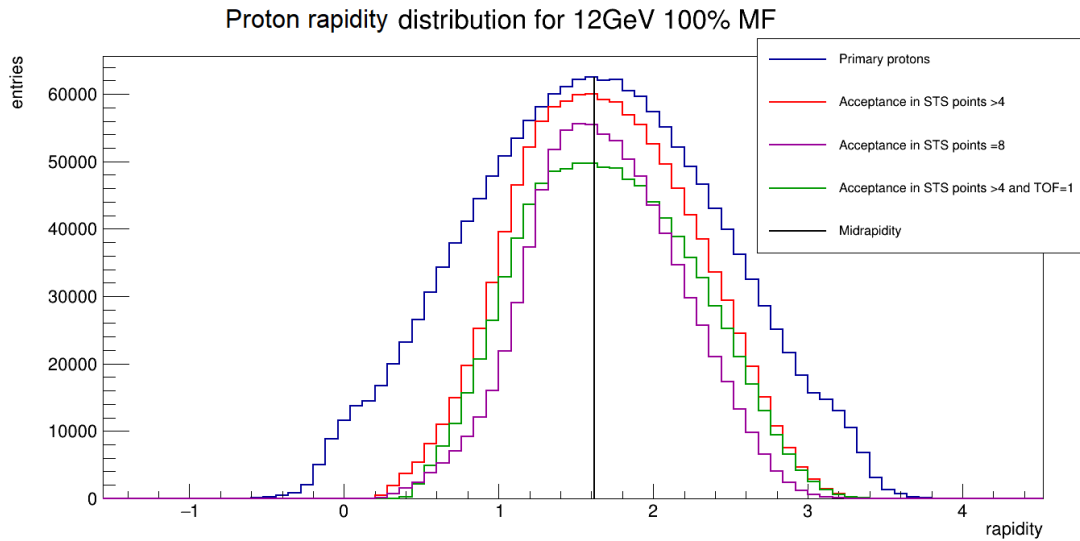


Figure 2.1: Rapidity distribution for 12GeV/u and 100 % magnetic field

Fig.2.1 shows thee rapidity distributions for 12 GeV/u beam momentum and 100% of mag-netic field with different acceptance criteria. The blue plot shows the distribution of all primary protons. The red one shows the distribution of all primary protons which have at least 4 STS points. Pink plot shows distribution of all primary protons which have all 8 STS points. The most important plot is the green plot. It shows distribution of all primary protons which have at least 4 STS points and 1 TOF point.

Fig.2.2 shows the same distributions for 4 GeV/u beam momentum and 100% of magnetic field. The distributions of accepted protons are shifted left relative to the midrapidity line.

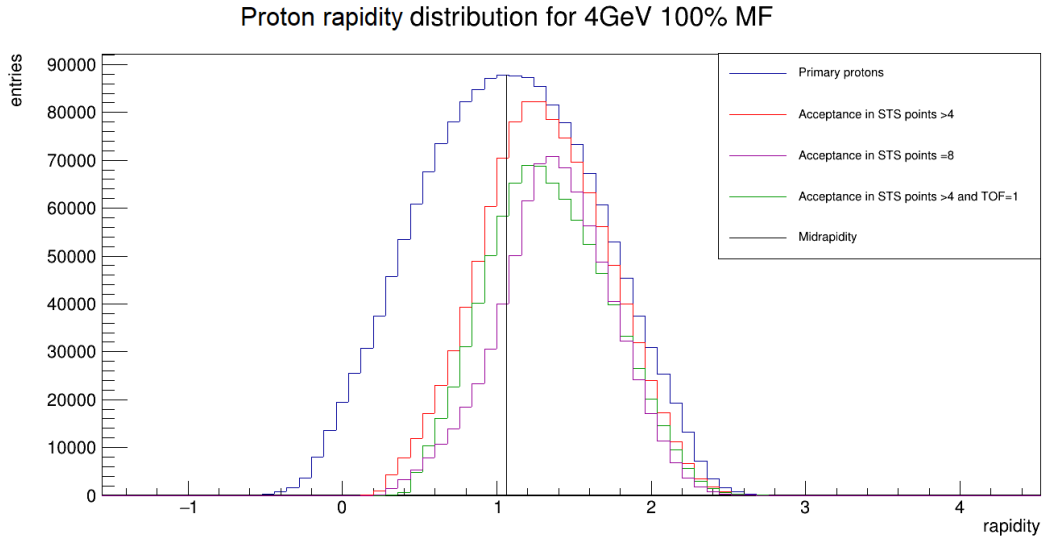


Figure 2.2: Rapidity distribution of protons for 4GeV/u and 100 % magnetic field

An assumption was made, that if we preserve the ratio of energy and magnetic field the rapidity distribution will shift towards the midrapidity line and be symmetrical with respect to it. To check that assumption rapidity distribution for 4GeV/u beam momentum and 33% magnetic field were calculated (Fig.2.3). Contrary to our expectation, the difference to 100 % of magnetic field is small.

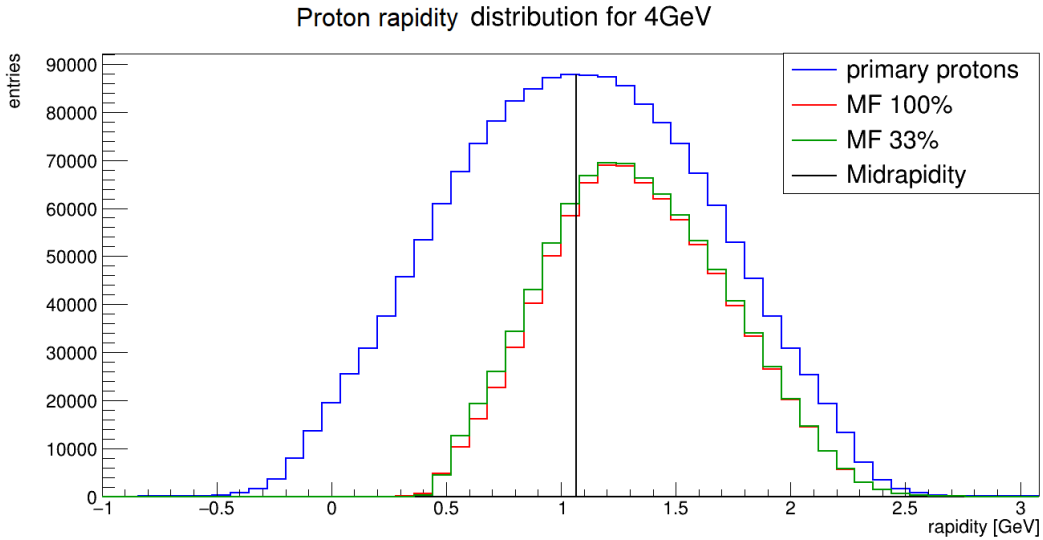


Figure 2.3: Rapidity distribution of protons accepted in STS and TOF for 4GeV/u and different magnetic field settings

Fig.2.4 shows the 2D distribution of accepted protons in transverse momentum and rapidity for 4GeV/u beam momentum and different magnetic field settings to see if a magnetic field change results in any change in distribution. Again, we do not see a major difference between the different magnetic field settings.

Next, we study the TOF acceptance, which is defined as the distribution of rapidity for particles having at least 4 STS points and 1 TOF point divided by the rapidity distribution

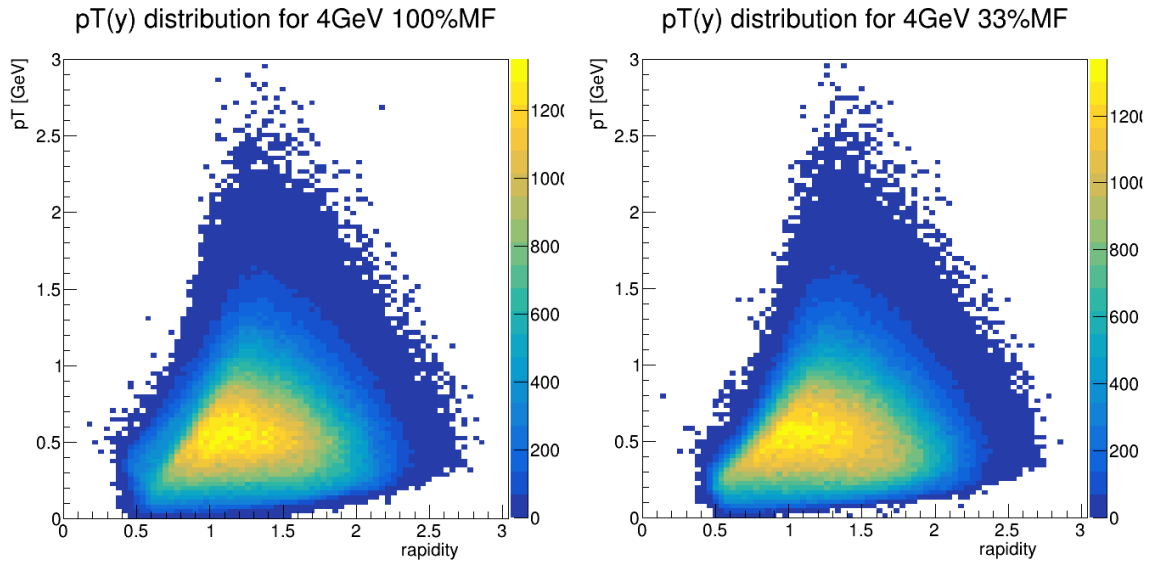


Figure 2.4: Distribution of accepted protons in transverse momentum and rapidity 4 GeV/u beam momentum and different magnetic field settings

for particles having at least 4STS points.

$$acceptance_{TOF} = \frac{y_{TS4+TOF1}}{y_{TS4}} \quad (2.2)$$

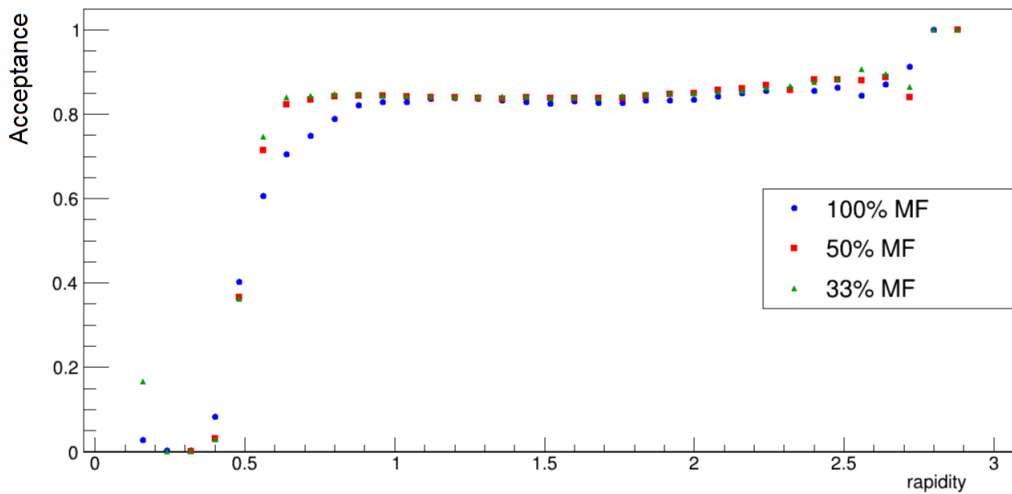


Figure 2.5: TOF acceptance for 4GeV/u beam momentum and different magnetic field settings

As Fig.2.5 shows, the magnetic field has impact on the acceptance for smaller rapidity values but not for rapidity higher than 1.

Chapter 3

Reconstruction efficiency

Another key figure is the reconstruction efficiency, i.e. the probability that a simulated track is found in the reconstruction procedure. We study the reconstruction efficiency as function of momentum for primary protons.

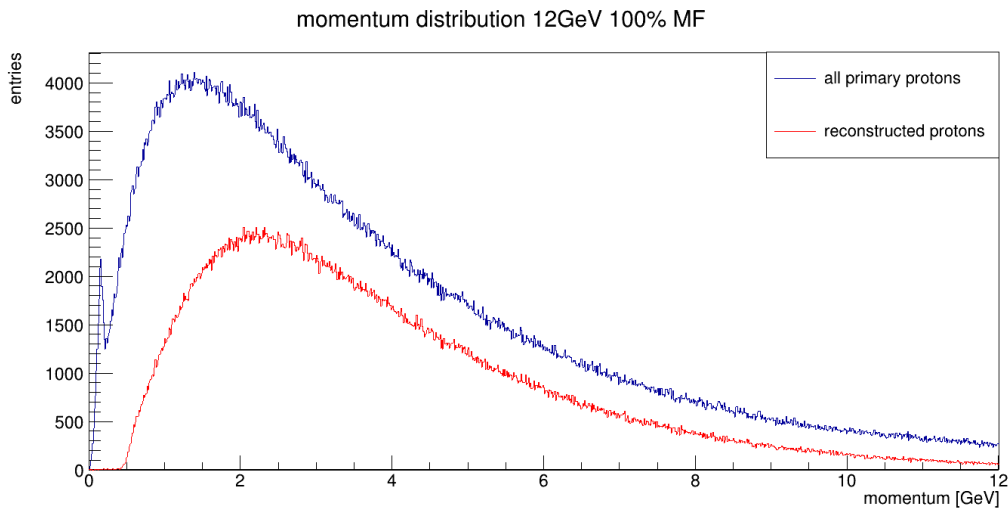


Figure 3.1: Momentum distribution for 12GeV/u beam momentum 100% magnetic field for all simulated primary protons and all reconstructed primary protons

Fig.3.1 shows momentum distribution for 12GeV/u beam momentum and 100% of magnetic field. The blue plot shows all primary protons got from simulation, while the red one shows momentum distribution for all reconstructed primary protons. Two plots shows the difference in number of simulated and reconstructed primary protons.

Fig.3.2 shows momentum distribution for 4 GeV/u and 100% of magnetic field. As one can see, for lower energies, distribution reaches lower momentum values.

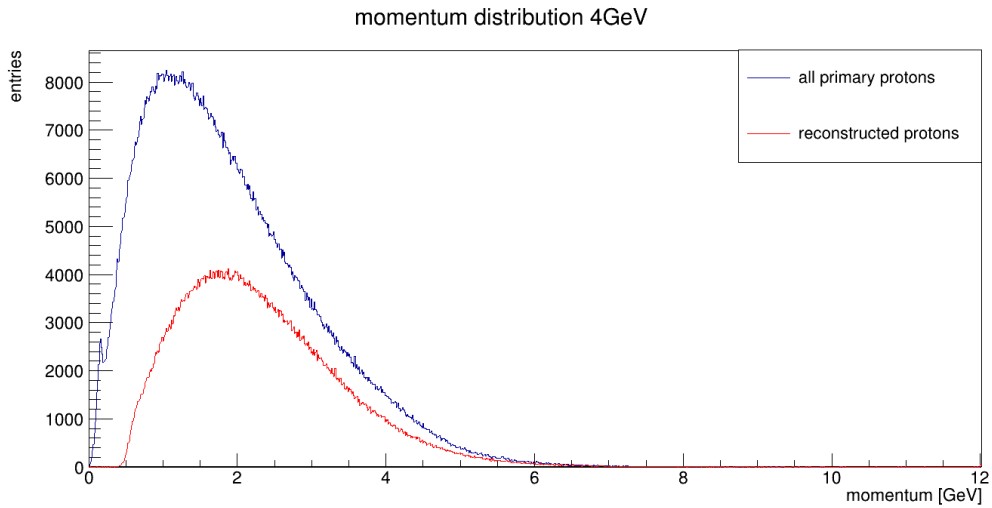


Figure 3.2: Momentum distribution for 4GeV/u beam momentum 100% magnetic field for all simulated primary protons and all reconstructed primary protons.

To check if changing magnetic field setting have any impact on the momentum distribution, plots for 4GeV/u beam momentum and different magnetic field for reconstructed primary protons were plotted (Fig.3.3). As one can see, for lower magnetic field setup the number of reconstructed primary protons gets slightly bigger.

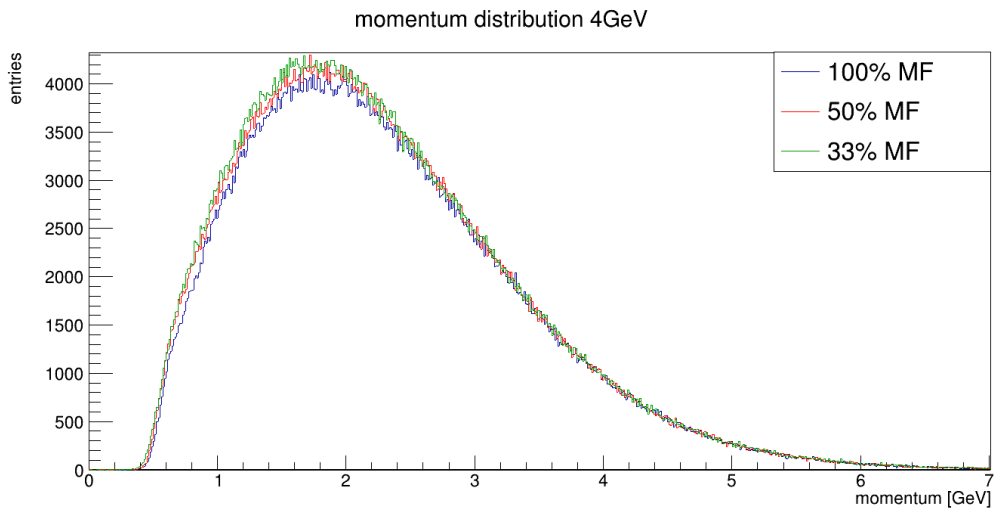


Figure 3.3: Momentum distribution for 4GeV/u beam momentum and different magnetic field settings for reconstructed primary protons

Chapter 4

Momentum resolution

The value called momentum resolution provides us with information of how big is the difference between momentum of the particle from simulation and momentum after reconstruction.

To begin with the 2D histogram of value called dp/p in function of momentum p was plotted.

$$\frac{dp}{p} = \frac{p_{MC} - p_{rec}}{p_{MC}} \quad (4.1)$$

dp/p is the difference subtraction result of momentum of the particle from simulation and momentum of the particle from reconstruction divided by momentum of the particle from simulation.

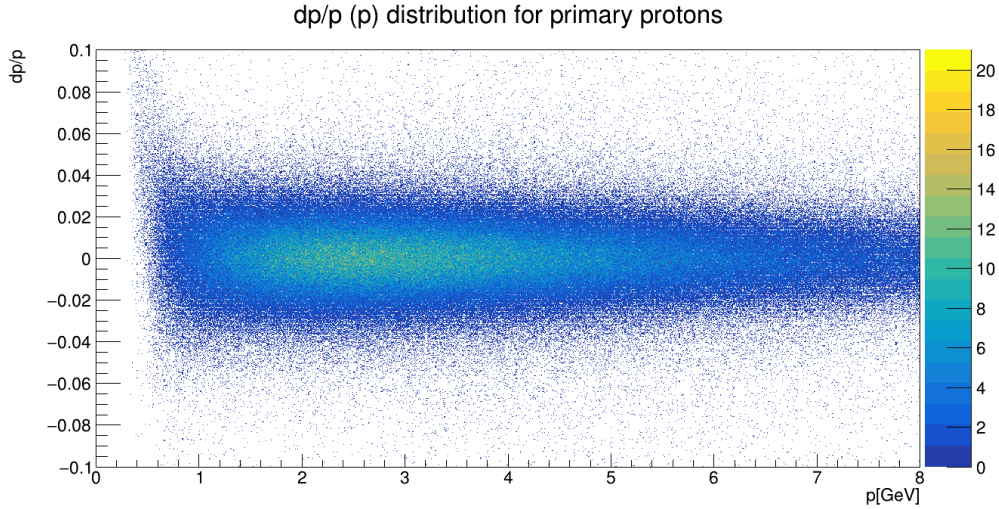


Figure 4.1: 2D histogram of dp/p in function of momentum for primary protons

By getting the projection of dp/p for every bin (showed in Fig.4.2) and fitting Gaussian distribution we can get standard deviation of the distribution at given p

Fig.4.3 shows the standard deviation as function of momentum from simulation for different beam momentum and 100% of magnetic field. The distributions are similar.

Fig.4.4 shows the standard deviation as function of momentum from simulation for 4GeV beam momentum and different magnetic field settings. As was expected, for lower magnetic field setups standard deviation gets bigger. It is strongly connected to the fact that magnetic field affects particle trajectory curvature.

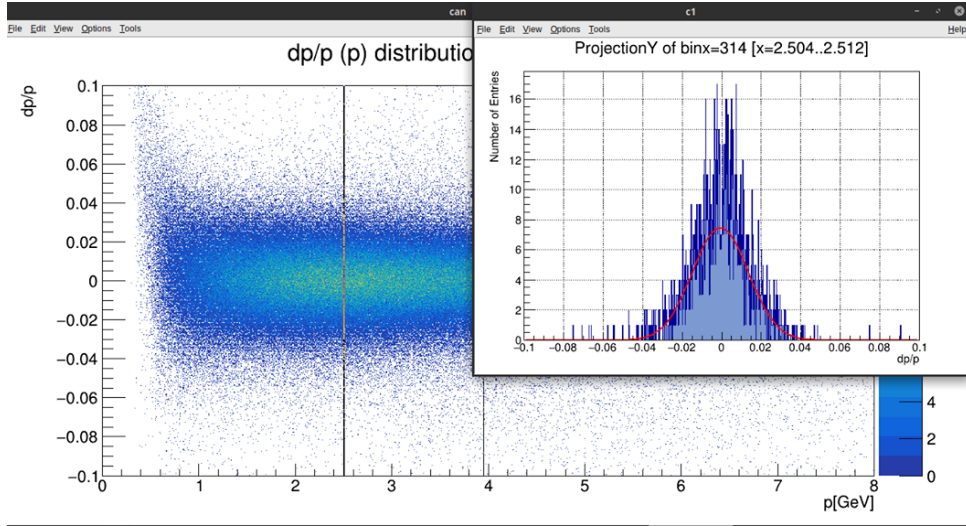


Figure 4.2: Example of projection of the $dp/p(p)$ distribution with Gaussian fit

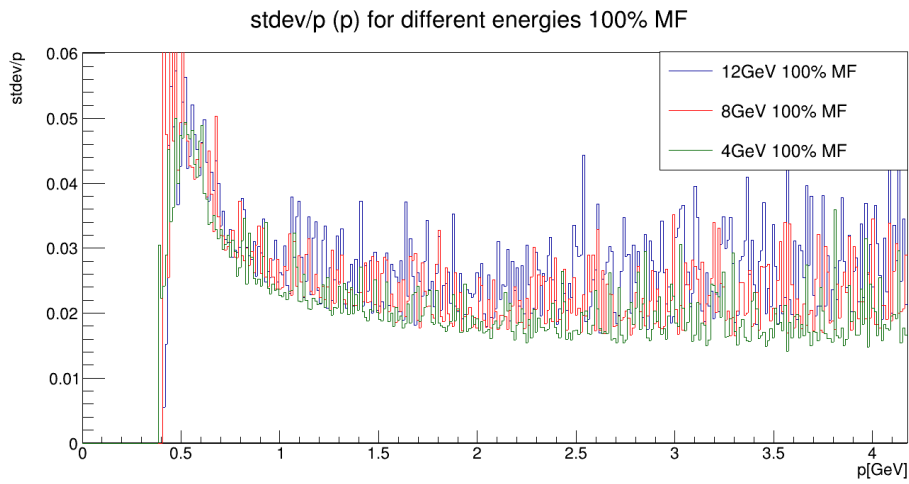


Figure 4.3: Relative momentum resolution as function of momentum for different beam momentum and 100% of magnetic field

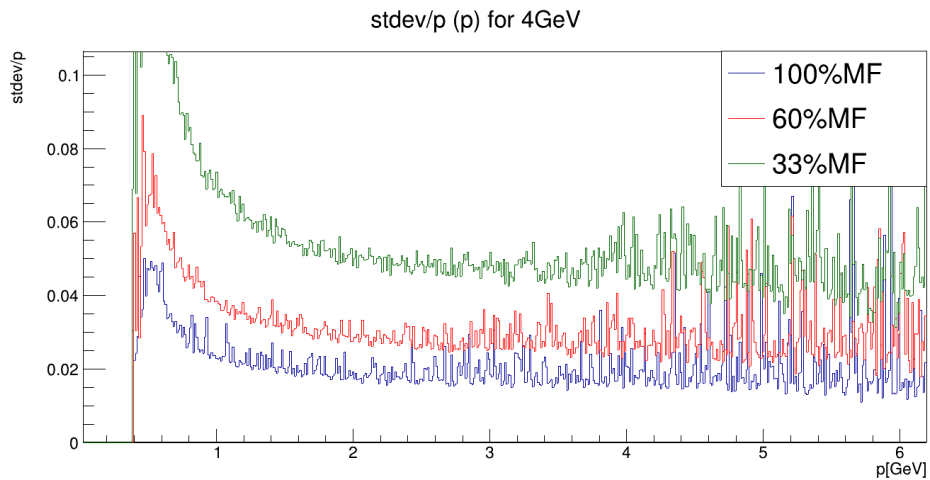


Figure 4.4: Relative momentum resolution as function of momentum for 4 GeV/u beam momentum and different settings of magnetic field

Chapter 5

Lambda reconstruction

Lambda is baryon which commonly decays to: proton p and pion- π^- or to neutron n and neutral pion π^0 .

The first pair of Lambda's daughters makes up the majority of lambda decays. Furthermore, in physics analysis we only take the first daughters pair as the candidates because both proton and pion- are charged particles and neutral particles are not detected by CBM.

Having two charged particles which can be taken as candidates for Lambda daughters we can get distribution of invariant mass. Invariant mass is defined as:

$$m_{inv} = \sqrt{(E_1 + E_2)^2 - (p_1 + p_2)^2} \quad (5.1)$$

, where E is the energy of daughter particle and p is the momentum.

Using data from Monte Carlo we can check if two particles: proton and π^- are secondary particles, are the result of decay of the same mother particle and if that particle is Lambda particle.

By implementing those conditions we can get the perfect histogram of Lambda mass containing only one bin in the place of Lambda mass (Fig.5.1).

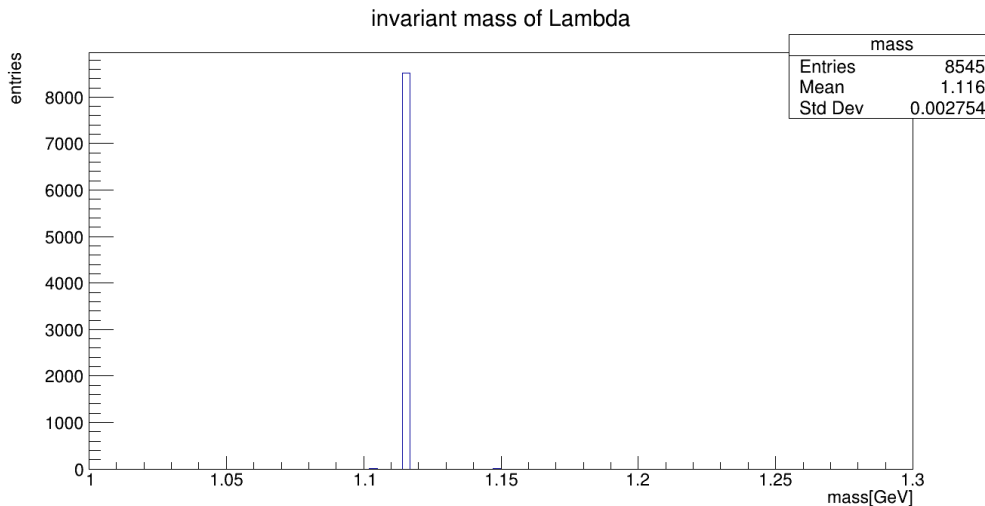


Figure 5.1: Distribution of invariant mass of Lambda with use of Monte Carlo data

In real experiment we have to implement different cuts. So by implementing them to reconstructed data we wanted to achieve a distribution similar to reconstruction from the real experiment.

The first cut that was implemented is the impact parameter in the target plane, which helps in distinguishing secondary particles from primary ones. To get the impact parameter we have

to extrapolate the trajectory of the particle (pion or proton) in the direction of the main vertex. The distance between the beam and trajectory for the same z position is the impact parameter (see Fig.5.2). The distributions of the impact parameter are shown in Fig.5.3 and Fig.5.4 for protons and pions.

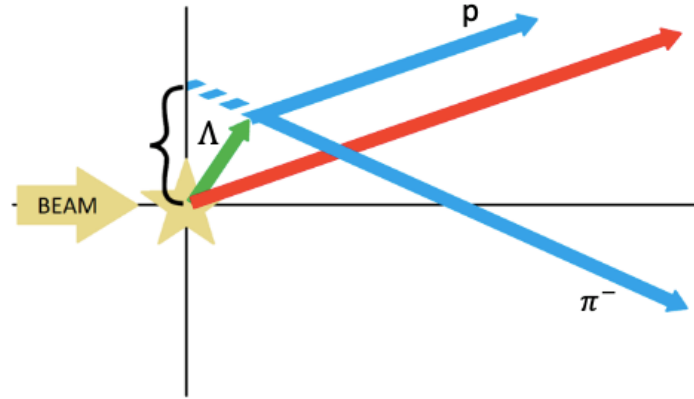


Figure 5.2: Impact parameter

They allow to define value of impact parameter after which we would get almost only the secondary particles. Implemented intervals: for protons impact parameter ≥ 0.2 cm and for pions impact parameter ≥ 0.6 cm.

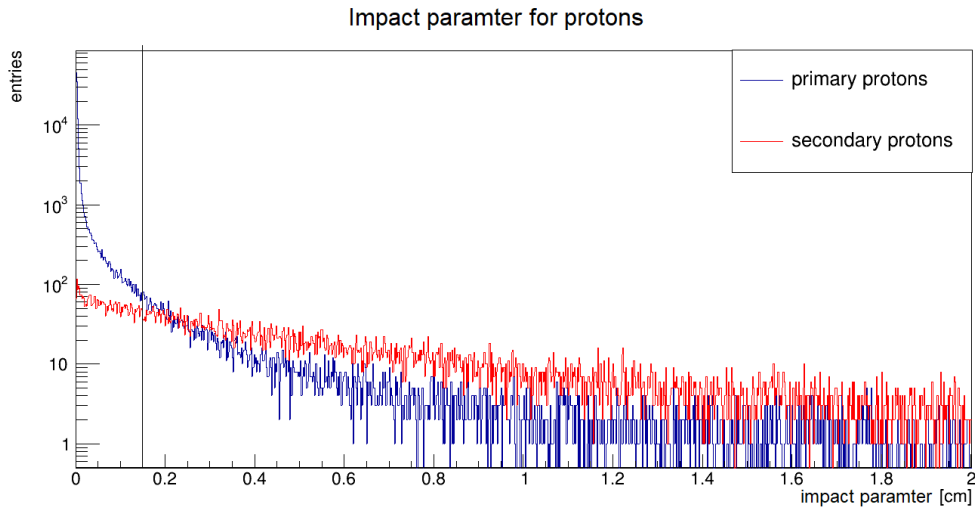


Figure 5.3: Impact parameter distribution for primary and secondary protons

For the identification of the Lambda daughters we study the $m^2(p)$ distribution (Fig.5.5). The following cuts were applied: for pions- $m^2 \in [0; 0.04]$ and for protons $m^2 \in [0.75; 1.0]$.

After implementing these cuts, the result was not satisfactory (Fig.5.6). The distribution of invariant mass has no visible peak in place of Lambda mass, there is a lot of background.

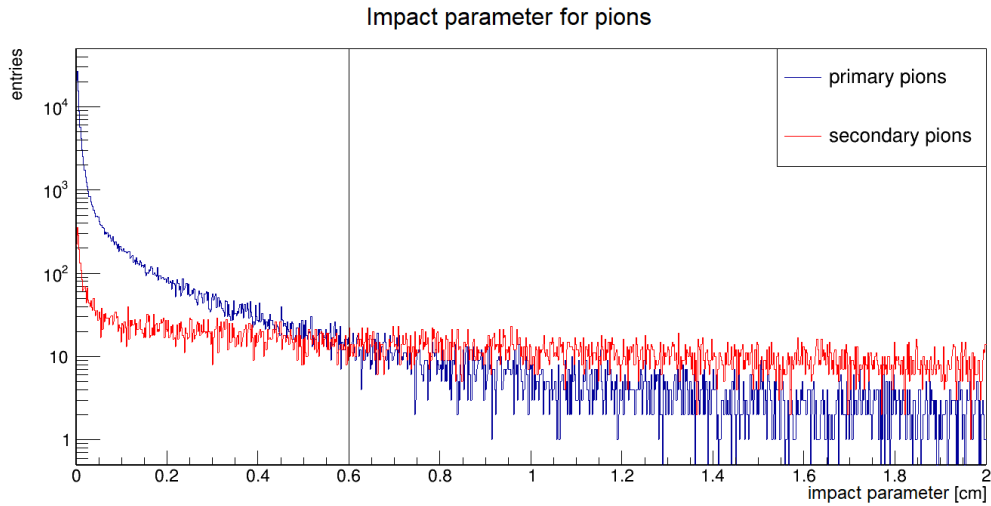


Figure 5.4: Impact parameter distribution for primary and secondary π^-

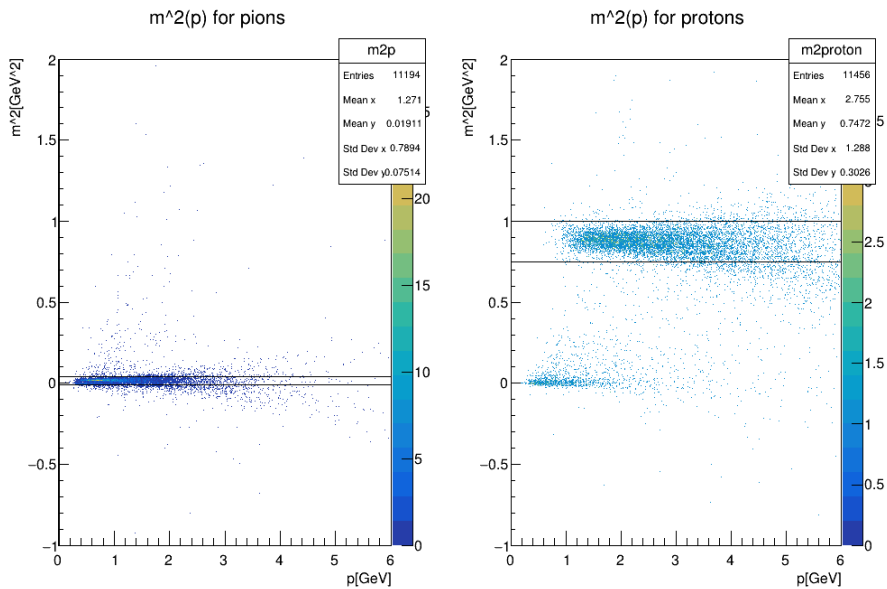


Figure 5.5: m^2 distribution as function of momentum for primary π^- and protons

While trying to find the cause of the problem we decided to use momentum values from Monte Carlo data and the result (Fig.5.7) is something we expected - there is a fair amount of noise, but we can see a clear peak in the place of the Lambda mass.

The reason for the unsatisfying result in Fig.5.6 is that the reconstructed momentum of the particles at the point of the first measurement was used. Because of the bending in the magnetic field this differs from the momentum vector at the decay point which is the correct one to be applied.

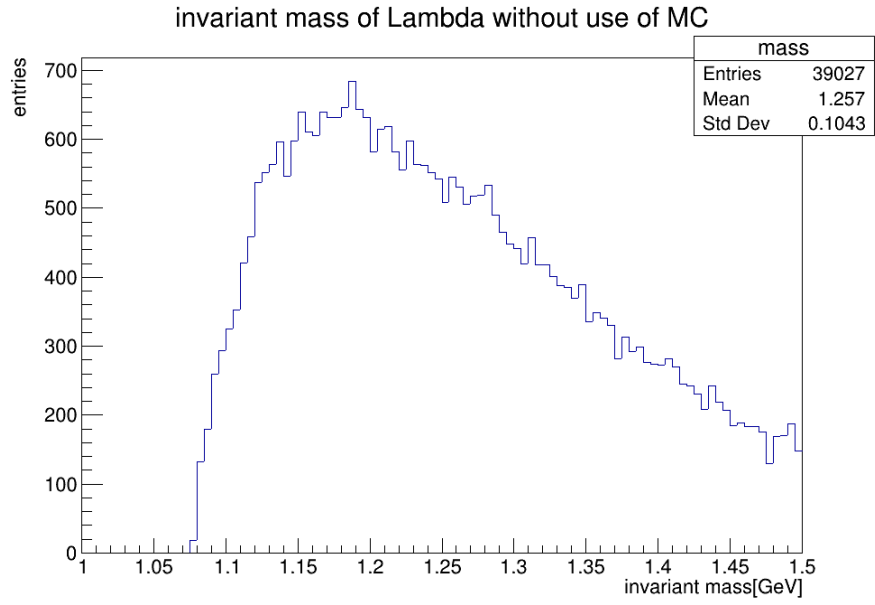


Figure 5.6: Distribution of invariant mass of $p\pi^-$ with the reconstructed momentum

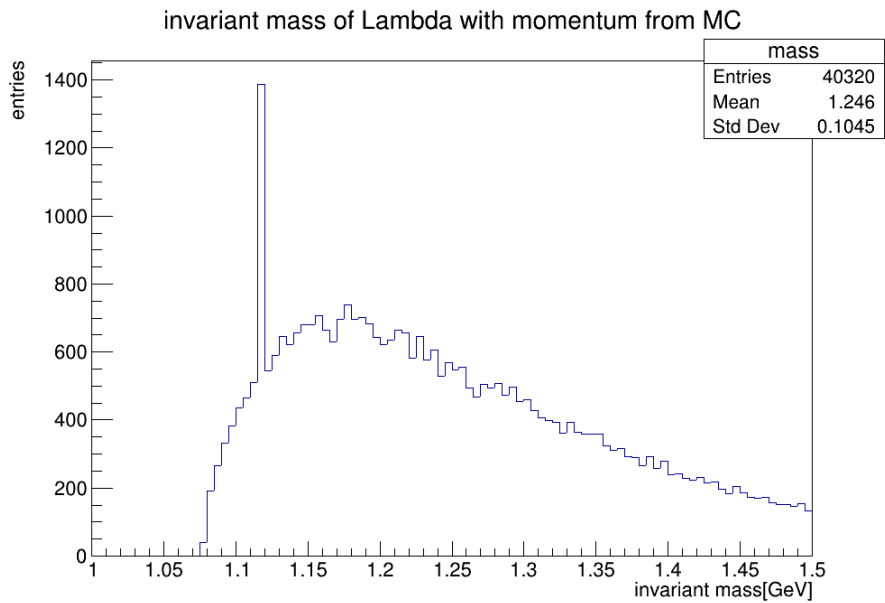


Figure 5.7: Distribution of invariant mass of $p\pi^-$ with Monte Carlo momentum values

Chapter 6

Lambda efficiency

In this part of the project the KFParticle Finder package was used. KFParticle Finder is the package that will be used in CBM Experiment, here at GSI. It provides us with a lot of information in form of already prepared histograms containing the distribution of invariant mass of Lambda and also with histograms containing only the separated Lambda peak, and only the separated background.

Efficiency is one of the main observables which we want to investigate. Efficiency of reconstructing Lambda is defined as:

$$efficiency_{KF} = \frac{\text{number of reconstructed Lambdas from KFParticle Finder}}{\text{number of lambdas from simulation}} \quad (6.1)$$

Additionally, to see the difference, the efficiency defined as number of Lambdas from reconstruction divided by number of lambdas from simulation was plotted (Fig.6.1).

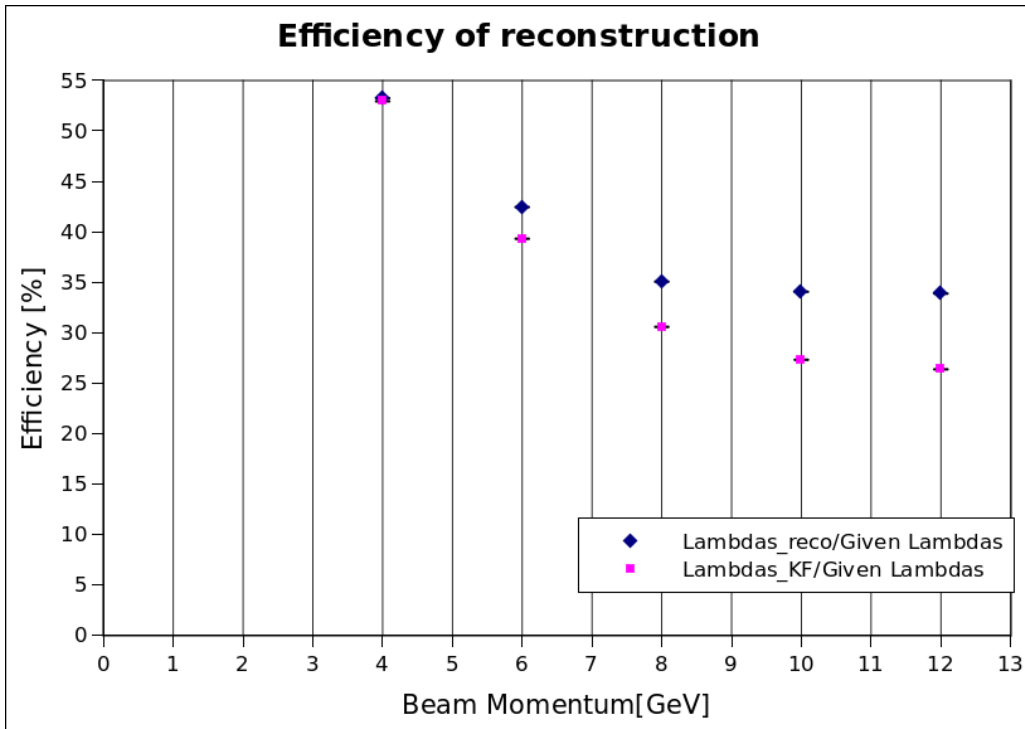


Figure 6.1: Efficiency of Lambda for different beam momentum and 100% of magnetic field

The efficiency decreases with beam momentum. To check if magnetic field setting has any impact on efficiency, the efficiency a function of magnetic field is shown in Fig.6.2 for 4GeV/u beam momentum. As one can see for lower magnetic field setting efficiency gets bigger.

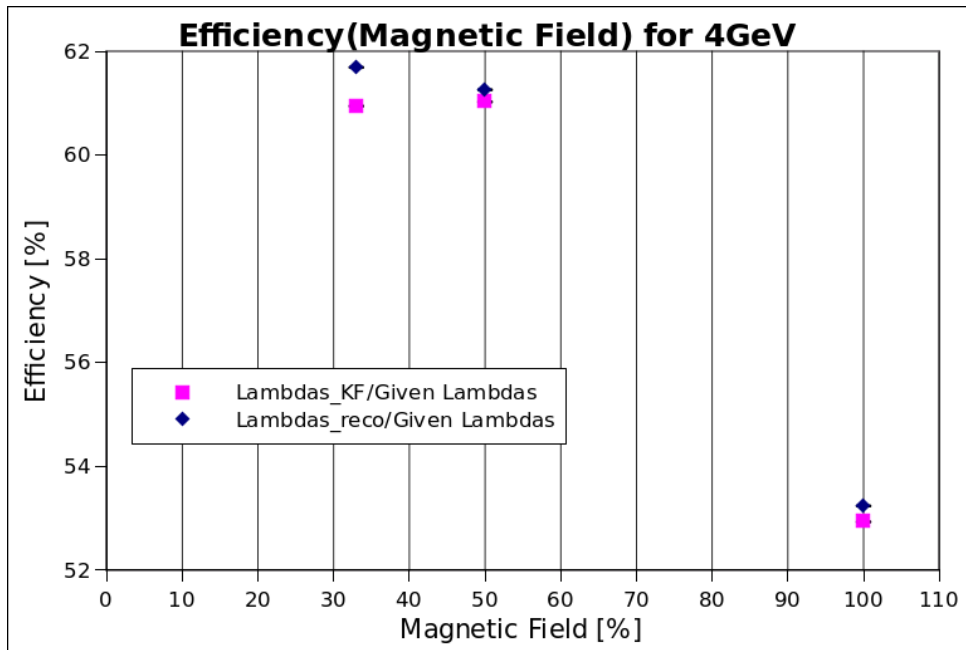


Figure 6.2: Efficiency of Lambda for 4GeV beam momentum and different magnetic field settings

The next main observable which we want to investigate is the width of the reconstructed Lambda peak. This values can be obtained by fitting a Gaussian distribution to the invariant mass of Lambda peak distribution, and taking the standard deviation of that fit (Fig.6.3). The smaller the value of the width gets the better, because the signal is then easier to separate from the background.

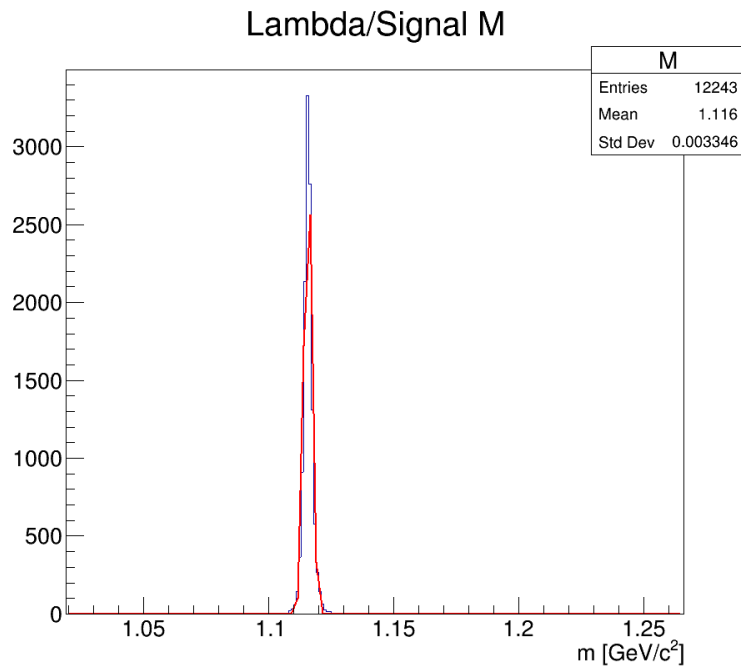


Figure 6.3: Reconstructed invariant mass of Lambda from KFParticle Finder with Gaussian fit

The width of the Lambda peak as function of beam momentum for different magnetic field setups is shown in Fig.6.4. A lower magnetic field results in larger width of the peak. For 100%

of magnetic field we see that the width stays constant with beam momentum. This is in line with our assumptions, as the width of reconstructed Lambda distribution is strongly connected to the magnetic field.

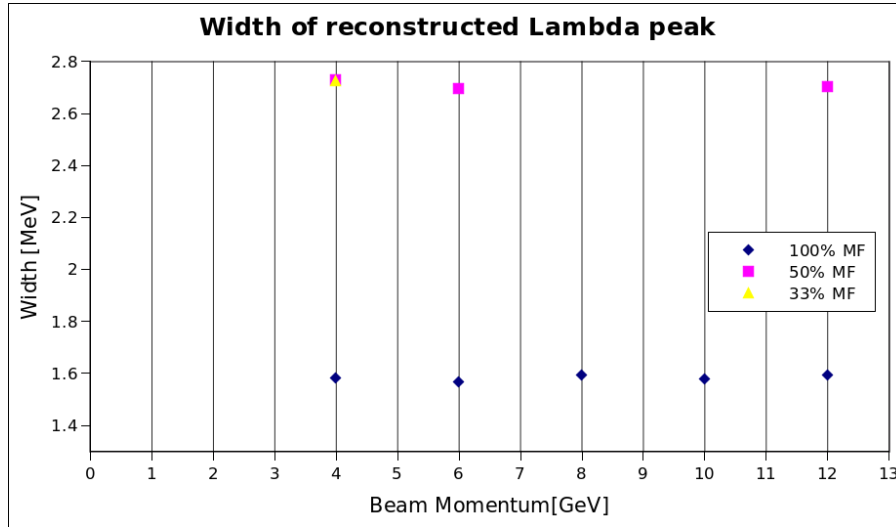


Figure 6.4: Width of the Lambda peak for different energies and different magnetic field settings

The last variable that needed to be investigated is the signal to background ratio. In Fig.6.5 we see the peak of reconstructed Lambda, which is our signal, and marked in red color part of the background, in the intervals designated by Lambda signal peak, which will be our background for further calculations.

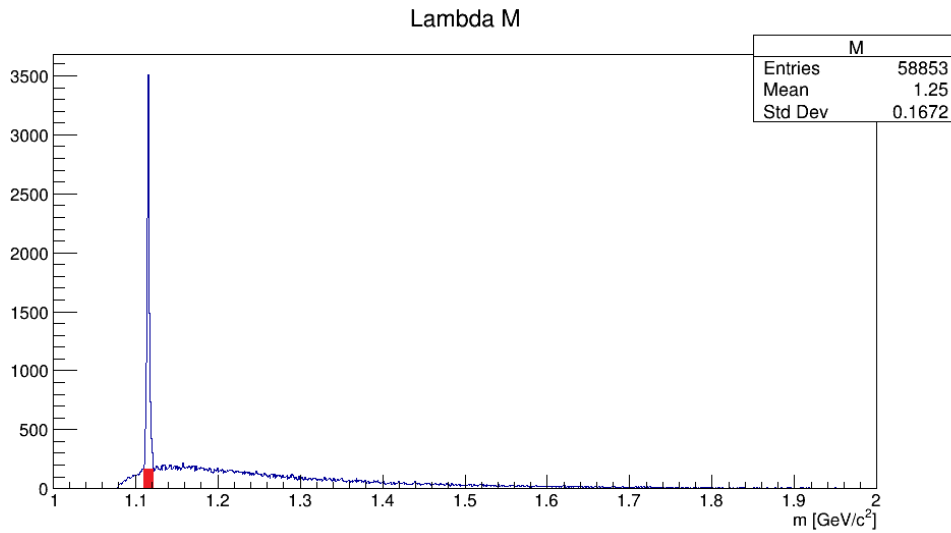


Figure 6.5: Distribution of invariant mass of $p\pi^-$ from KFParticle Finder. The marked area under the peak is the background used for calculating the signal-to-background ratio.

The signal to background ratio as function of beam momentum is showed in Fig.6.6 for different magnetic field settings. In principal, what can be spotted is that he ratio gets smaller for larger beam momentum, and also is approaching unity for smaller magnetic field settings. This is something that we expected, as for smaller magnetic field the reconstruction is worse, the background gets bigger and the reconstructed peak of invariant mass of Lambda is smaller. As the signal and the background reach similar values the ratio approaches unity.

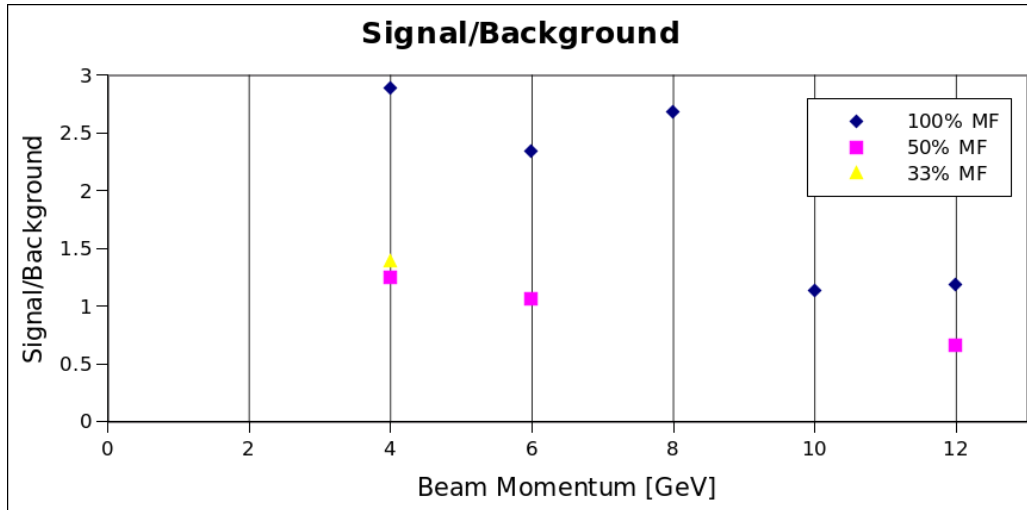


Figure 6.6: Signal to background ratio as function of beam energy for different magnetic field settings

Chapter 7

Conclusion

We have studied the impact of the magnetic field settings for key performance figures of CBM. Our findings are:

- We observe only a small influence of the magnetic field on the geometrical acceptance of primary protons.
- The momentum resolution increases from about 2% to about 5% when reducing the magnetic field by a factor of 3 for 4GeV/u beam momentum.
- Λ reconstruction necessitates the extrapolation of the reconstructed momentum to the decay point.
- For full magnetic field, the Λ reconstruction efficiency drops from 53% at 4GeV/u to 35% at 12GeV/u beam momentum. At 4GeV/u it increases to 61% for reduced magnetic field.
- The width of the Λ peak increases from 1,6MeV to 2,7MeV when reducing the field by a factor of 2. Consequently the signal-to-background ratio is reduced by a similar factor.

Bibliography

- [1] <https://fair-center.eu/for-users/experiments/cbm-and-hades/cbm.html>
- [2] "Challenges in QCD matter physics- The scientific programme of the Compressed Baryonic Matter experiment at FAIR" T.Abliczymov et al. (CBM Collaboraion), Eur.Phys.J.A53 (2017)60
- [3] <http://home.agh.edu.pl/kakol/efizyka/w22/main22c.html>